Supporting Information

Morairty et al. 10.1073/pnas.1314762110

SI Materials and Methods

Animals. A total of 75 male Sprague-Dawley rats (300 ± 25 g at time of surgery; Charles River) were distributed among the 15 groups described under "Experimental Protocols" below. Thirteen male B6;129S4-Nos1$^{tm1\ Plh}$ neuronal nitric oxide synthase (nNOS) null mutant (nNOS KO) and 17 B6;129SF2/J WT mice (Jackson Laboratories) were separated into two groups for either telemetric or tethered EEG recordings (see below). All animals were housed in separate cages in a temperature-controlled recording room (24 ± 2 °C, 50% ± 20% relative humidity) under a 12 h/12 h light/dark cycle and had food and water available ad libitum. All experimental procedures involving animals were approved by SRI International's Institutional Animal Care and Use Committee and were in accordance with National Institutes of Health guidelines.

Surgical Procedures. Surgical procedures for rats involved implantation of sterile telemetry transmitters (F40-EET, Data Sciences Inc.) as previously described (1, 2).

Two types of surgical procedures were conducted in mice. Procedures for implantation of telemetry transmitters (F20-EET, Data Sciences Inc.) for chronic recording of EEG and electromyography (EMG) were similar to those described previously (3). Under isofluorane anesthesia, midline cranial and abdominal incisions were made, and transmitters were placed IP along the midline and anchored to the abdominal wall. Biopotential leads were routed s.c. to the head and neck. After the abdominal incision was closed, cranial holes were drilled 1 mm anterior to bregma and 1 mm lateral to midline and, contralaterally, 2 mm posterior to bregma and 2 mm lateral to midline. EEG leads were wedged subcranially over the dura and were attached to the skull with cyanoacrylate and dental acrylic. EMG leads were positioned bilaterally through the nuchal muscles and were anchored with polyamide 4-0 suture. The cranial incision was closed, and the mice were administered postoperative analgesics and hydration s.c. (buprenorphine, 0.05–0.1 mg/kg and ketoprofen, 2–5 mg/kg, 0.7 mL lactated Ringers solution), thermal support, and soft chow for at least 2 d.

Conventional tethered EEG and EMG recordings were as described in detail elsewhere (4). Prefabricated headmounts (Pinnacle Technologies) were implanted under general anesthesia in sterile conditions. The headmount (three channels: two EEG and one EMG) was affixed to the skull using cyanoacrylate and stainless steel screws (0.10" and 0.12") that contacted the dura and also functioned as EEG electrodes. The front edge of the headmount was placed 3.0 mm anterior to bregma aligned centrally along the sagittal suture. In this configuration, EEG electrodes were positioned 1.5 mm lateral to the sagittal suture, 2.0 mm anterior of bregma, and −4.0 mm posterior to bregma. The threads of the EEG electrodes were coated with silver epoxy (Pinnacle Technologies) to ensure a solid connection with the headmount. EMG electrodes attached to the headmount were inserted into the trapezius muscle and sutured in place. The implant was secured to the cranium using dental acrylic (Lang Dental Manufacturing Co.), and the incision was closed. For 1 to 2 d after surgery, mice were administered analgesics, hydration, thermal support, and soft chow as described above.

All animals were allowed a minimum of 3 wk recovery from surgery before any experimental procedures or recordings. Animals were maintained in their home cages during this recovery period. All subsequent EEG/EMG recordings, including tethered recordings, occurred in the animal's home cage.

Experimental Protocols. ***Protocol 1: Fos expression in cortical nNOS neurons associated with spontaneous sleep/wake.*** Because the major sleep period for the rat is shortly after light onset, homeostatic sleep drive should decrease across the 6-h period from Zeitgeber Time (ZT)4 to ZT10. Thus, in this experiment, rats were undisturbed while EEG and EMG were recorded, and animals were killed at ZT4 ($n = 5$), 6 ($n = 4$), 8 ($n = 4$), 9 ($n = 4$), or 10 ($n = 8$), perfused, and the brains prepared for double-label immunohistochemistry as described below.

Protocol 2: Assessment of the effect of sleep deprivation duration on Fos expression in cortical nNOS neurons. In this experiment, we varied the intensity of homeostatic sleep drive by depriving rats of sleep for 2 h ($n = 5$), 4 h ($n = 3$), or 6 h ($n = 6$) beginning at light onset and then allowing a 2-h recovery sleep (RS) opportunity. Because this protocol necessitated that the rats were killed at different times of day, we compared these animals with the non-sleep deprived, time-matched controls described in Protocol 1. Thus, the experimental rats were killed at the end of the RS period (ZT4, -6, or -8), perfused, and the brains prepared for double-label immunohistochemistry as described below. In addition, one group of rats underwent a 2-h sleep deprivation (SD) followed by 4-h RS before killing ($n = 2$) and was thus killed at ZT6. The data from this group are only included in the correlational analyses (Figs. 2 and 3).

Protocol 3: Assessment of the effect of the RS duration on Fos expression in cortical nNOS neurons. Here, we assessed the time course of Fos expression in rats that were deprived of sleep for 6 h and then allowed an RS opportunity of either 0 ($n = 4$), 30 ($n = 6$), 60 ($n = 6$), 90 ($n = 6$), 120 ($n = 6$; described in protocol 2), 180 ($n = 6$), or 240 ($n = 6$) min. To ensure that homeostatic sleep drive was comparable across groups, SD began at light onset for all groups, which meant that the time of killing varied from ZT6 to ZT10 in this experiment.

SD Procedures. SD procedures were similar to those previously published (5, 6). Animals were continuously observed and, when inactive and appeared to be entering sleep, cage tapping occurred. As SD progressed and it became more difficult to sustain wakefulness, novel objects were introduced into the home cage, and, when necessary, an artist's brush was used to stroke the fur or vibrissae.

Multiple Sleep Latency Test. To objectively measure sleepiness, we performed a variation of the murine Multiple Sleep Latency Test (7) with 7 nNOS KO and 11 WT mice. Starting 3 h into the light period, mice were subjected to five 20-min sessions of forced waking, each followed by a 20-min nap opportunity within a continuous 200-min time interval. The latency to the onset of non-rapid eye movement (NREM) and rapid eye movement (REM) sleep as well as the percentage of time spent in both states was determined for each nap opportunity.

Identification of Sleep/Wake States and Sleep/Wake Data Analyses. After 3 wk postsurgical recovery, EEG, EMG, body temperature, and locomotor activity were recorded via telemetry using DQ ART 4.1 software (Data Sciences Inc.). For tethered recordings, EEG and EMG signals were collected using a Neurodata model 15 data amplifier system (Grass-Telefactor), digitized, and stored on a computer using VitalRecorder software (Kissei Comtec). After completion of the data collection, expert scorers determined states of sleep and wakefulness in 10-s epochs by examining the recordings visually using NeuroScore software

(Data Sciences Inc.). The EEG and EMG data were scored for waking, REM, and NREM. As indices of the consolidation of behavioral states, the average duration and number of bouts for each state were calculated. A "bout" consisted of a minimum of two consecutive 10-s epochs of a given state and ended with any single state change epoch. EEG spectra during NREM sleep were analyzed offline by fast Fourier transform algorithm using a Hanning Window (NeuroScore software, Data Sciences Inc.) on all epochs without artifact. EEG δ power (0.5–4.5 Hz) within NREM (NRD) was then calculated. Raw NRD was normalized to 2 h of an undisturbed baseline recording from ZT5 to ZT7 on a previous day. Because three rats had corrupted baseline recordings, they were therefore excluded from analyses of normalized spectra. Normalized NRD energy was calculated by multiplying the time (h) spent in NREM sleep by the normalized NRD power.

Immunohistochemistry and Cell Counts. Brain sections were cut at 40-μm thickness. Double-labeled immunohistochemistry for Fos and nNOS was performed on serial sections of rat brain as described previously (8, 9). Sections were first incubated overnight with rabbit anti-Fos antibody (1:2,000, sc-52, Santa Cruz Biotechnology), then with biotinylated donkey anti-rabbit antibody (1:500, Jackson ImmunoResearch), followed by avidin-biotinylated horseradish peroxidase complex (1:200, PK-6100, Vector Laboratories), and nickel-enhanced 3,3′ diaminobenzidine (SK4100, Vector Laboratories) for a black reaction product. Subsequently, sections were incubated overnight in mouse anti-nNOS antibody (N2280, Sigma-Aldrich), then with biotinylated donkey anti-mouse antibody, followed by avidin-biotinylated alkaline-phosphatase complex (AK-5000, Vector Laboratories), and Vector Red reaction (SK-5100, Vector Laboratories) for a red reaction product. Single-labeled nNOS and double-labeled Fos^+/nNOS cells were counted in two hemisections of the cerebral cortex between 2.8 and 3.8 mm posterior to bregma, and the percentage of nNOS neurons expressing Fos was calculated as described previously (8, 9). For mice, sections were first stained for Fos as described above for rats. Subsequently, they were incubated overnight in rabbit anti-neurokinin-1 (NK1) antibody (1:1,000, gift from Ryuichi Shigemoto, IST Austria, Klosterneuburg, Austria), then with biotinylated donkey anti-rabbit antibody (1:500, Jackson ImmunoResearch), followed by avidin-biotinylated horse radish peroxidase complex (1:200, Vector Laboratories), and Nova Red reaction (SK-4805, Vector Laboratories) for a red-brown reaction product. Single-labeled NK1 and double-labeled Fos^+/NK1 cells were counted in two hemisections of the cerebral cortex, one at +0.9 to +1.1 mm and one at −1.2 to −1.7 mm from bregma, and the percentage of NK1 neurons expressing Fos was calculated.

Statistical Analyses. Groups were compared by two-tailed *t* tests or one-way or two-way ANOVAs followed by Holm-Sidak post hoc testing using SigmaPlot (Systat). When assumptions of normality or equality of variance were violated, a Kruskal-Wallis test followed by Bonferroni-Dunn post hoc testing was applied instead of one-way ANOVA. When equal variance or normality was violated for two-way ANOVA, *P* values for main effects and interactions were determined with permutation tests (10) with 5,000 iterations. Spearman rank correlations (r_s) were computed using the NaN toolbox (v2.0, http://biosig-consulting.com/matlab/NaN/) in Matlab 7.11.00 (MathWorks). In Fig. 2, exponential growth or exponential growth to maximum functions were fitted to correlation data using SigmaPlot. For comparison of EEG power spectra, two-way mixed-model ANOVAs were performed first as an omnibus test. When significant interactions were found, single bins were compared between genotypes using *t* tests (11).

1. Morairty SR, Hedley L, Flores J, Martin R, Kilduff TS (2008) Selective 5HT2A and 5HT6 receptor antagonists promote sleep in rats. *Sleep* 31(1):34–44.
2. Morairty SR, et al. (2012) Dual hypocretin receptor antagonism is more effective for sleep promotion than antagonism of either receptor alone. *PLoS ONE* 7(7):e39131.
3. Black SW, et al. (2013) Almorexant promotes sleep and exacerbates cataplexy in a murine model of narcolepsy. *Sleep* 36(3):325–336.
4. Fisher SP, et al. (2013) Longitudinal analysis of the EEG and sleep phenotype in the R6/2 mouse model of Huntington's disease. *Brain* 136(Pt7):2159–2172.
5. Terao A, et al. (2000) Prepro-hypocretin (prepro-orexin) expression is unaffected by short-term sleep deprivation in rats and mice. *Sleep* 23(7):867–874.
6. Terao A, et al. (2003) Differential increase in the expression of heat shock protein family members during sleep deprivation and during sleep. *Neuroscience* 116(1): 187–200.
7. Veasey SC, Yeou-Jey H, Thayer P, Fenik P (2004) Murine Multiple Sleep Latency Test: Phenotyping sleep propensity in mice. *Sleep* 27(3):388–393.
8. Gerashchenko D, et al. (2008) Identification of a population of sleep-active cerebral cortex neurons. *Proc Natl Acad Sci USA* 105(29):10227–10232.
9. Pasumarthi RK, Gerashchenko D, Kilduff TS (2010) Further characterization of sleep-active neuronal nitric oxide synthase neurons in the mouse brain. *Neuroscience* 169(1):149–157.
10. Manly BFJ (2007) *Randomization, Bootstrap and Monte Carlo Methods in Biology* (Chapman & Hall/CRC, Boca Raton, FL), 3rd Ed, p 461.
11. Vassalli A, et al. (2013) Electroencephalogram paroxysmal θ characterizes cataplexy in mice and children. *Brain* 136(Pt 5):1592–1608.

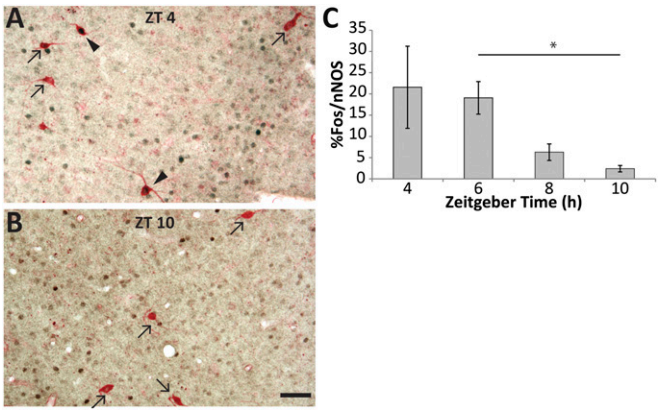

Fig. S1. Spontaneous activation of cortical nNOS neurons decays during the inactive period in undisturbed rats. (*A*) Representative micrograph of cortical nNOS neurons (red) of a rat killed at ZT4. Two of the five depicted neurons coexpress Fos (black). Arrows indicate single-labeled nNOS neurons, whereas arrowheads indicate double-labeled Fos^+/nNOS cells. (*B*) Representative micrograph of cortical nNOS neurons of a rat killed at ZT10. None of the four depicted cells is colabeled for Fos. (*C*) Percentage of cortical nNOS neurons found to coexpress Fos in rats killed at four times during the inactive period (protocol 1). $*P < 0.05$ for Bonferroni-Dunn post hoc test after significant Kruskal-Wallis test. (Scale bar, 50 μm.)

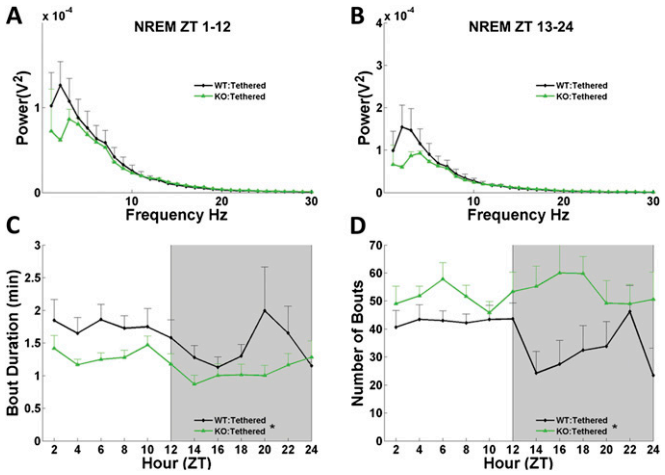

Fig. S2. Tethered recordings of nNOS KO and WT mice replicate the key findings from telemetric recordings. (*A*) NREM power spectra of nNOS KO and WT mice during the light phase. (*B*) NREM power spectra of nNOS KO and WT mice during the dark phase. Compare *A* and *B* with Fig. 3*D*. Although ANOVA failed to find significant differences between the genotypes, a tendency toward less power in the low δ range of KO mice (green traces) is apparent in *A* and *B*. (*C*) Average NREM bout duration across the 24-h period. Gray shading indicates dark period. Similar data from telemetry recordings presented in Fig. S3*C*. (*D*) Number of NREM bouts across the 24-h period. Shaded areas indicate lights-off periods. $*P < 0.05$ for main effect "genotype" in two-way mixed-model ANOVA.

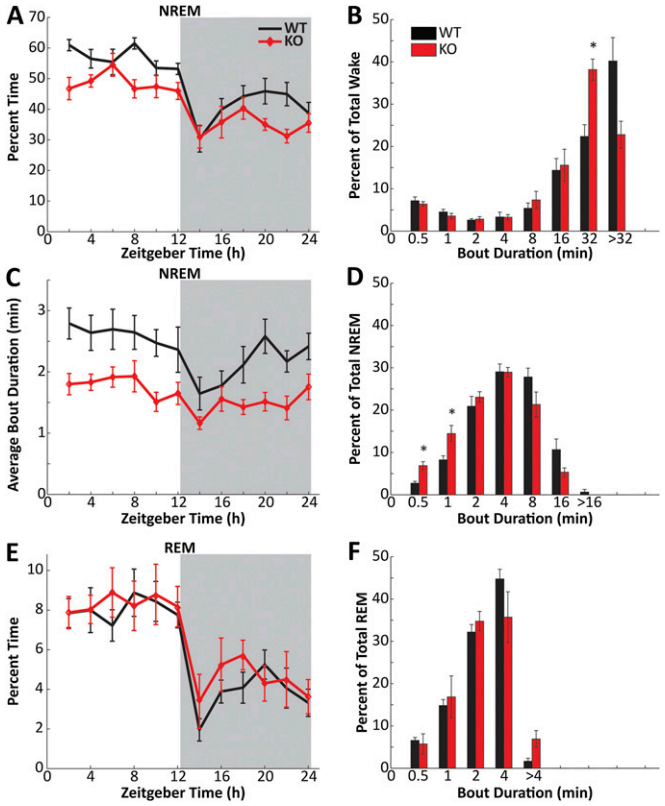

Fig. S3. Diurnal distribution of sleep parameters and sleep/wake bout duration frequency histograms from nNOS KO and WT mice. (*A*) Time spent in NREM across 24 h in nNOS KO and WT mice. (*B*) Time-weighted frequency histogram showing the proportion of time spent in wake in bouts of various durations. Labels on the abscissa indicate the maximum duration of the bouts represented in that bin. nNOS KO mice (red) spent more wake time in bouts of 16–32 min in duration, whereas WT mice spent ∼40% of the total time awake in bouts longer than 32 min. (*C*) Average NREM bout durations across 24 h. (*D*) NREM bout duration histogram. nNOS KO mice spent more NREM time than WT mice in short bouts up to 1 min in duration. (*E*) Time spent in REM across 24 h. (*F*) REM bout duration histogram. No significant interaction was found between genotype and REM bout durations. $*P < 0.05$ for Holm-Sidak post hoc test after significant interaction of factors "genotype" and "bout duration" was revealed by mixed-model permutation ANOVA.

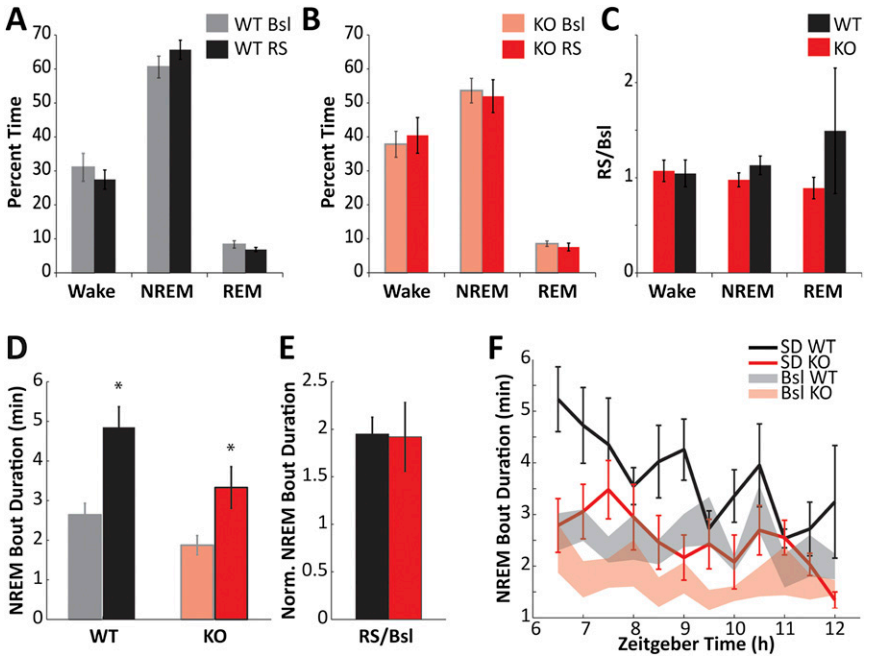

Fig. S4. State amounts and NREM bout duration in response to 6 h sleep deprivation in nNOS KO and WT mice. (*A* and *B*) Time spent in wake, NREM, and REM sleep during the 90-min RS opportunity and the corresponding baseline period for (*A*) WT mice and (*B*) KO mice. (*C*) Time spent in wake, NREM, and REM sleep during the 90-min recovery period relative to corresponding baseline period for WT (black) and KO mice (red). (*D*) NREM bout duration in the 90 min after 6 h SD (saturated colors) and the corresponding 90 min interval on the baseline day (light colors). Mixed-model ANOVA revealed main effects for genotype ($F_{1,18} = 4.65$, $P = 0.045$) and condition ($F_{1,18} = 34.86$, $P < 0.001$) but no interaction ($F_{1,18} = 1.48$, $P = 0.24$). *$P < 0.05$, Holm-Sidak post hoc test recovery sleep vs. baseline. (*E*) Same data as *D*, depicted as ratio of the RS 90 min to the baseline (Bsl) 90 min. (*F*) Time course of the average bout duration after 6 h SD.

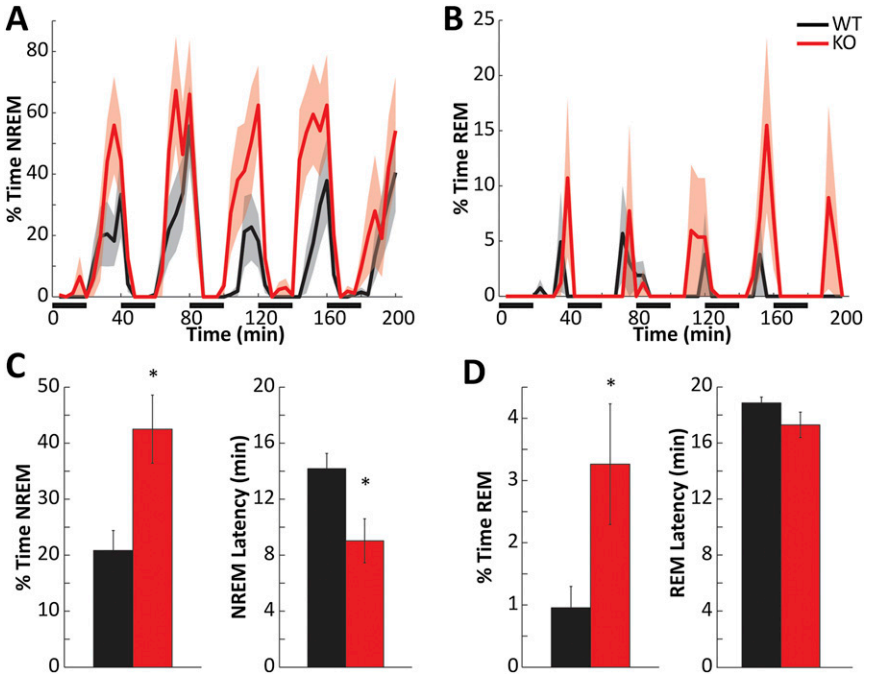

Fig. S5. nNOS null mutant mice are sleepier than WT mice in the murine Multiple Sleep Latency Test. (*A*) Percentage (±SEM) of NREM sleep observed in WT (black) and nNOS KO (red) mice during five 20-min "nap opportunities" after five 20-min periods of SD indicated by the horizontal bars below the abscissa. nNOS KO mice consistently had more NREM than WT mice. (*B*) Percentage of REM sleep observed in WT and nNOS KO mice during the five 20-min "nap opportunities" described in *A*. (*C*) Total time spent in NREM was greater and the latency to NREM was shorter in nNOS KO mice. (*D*) Although nNOS KO mice spent more time in REM sleep during the nap opportunities, the latency to REM did not differ between the two strains. *$P < 0.05$ for *t* test against WT.

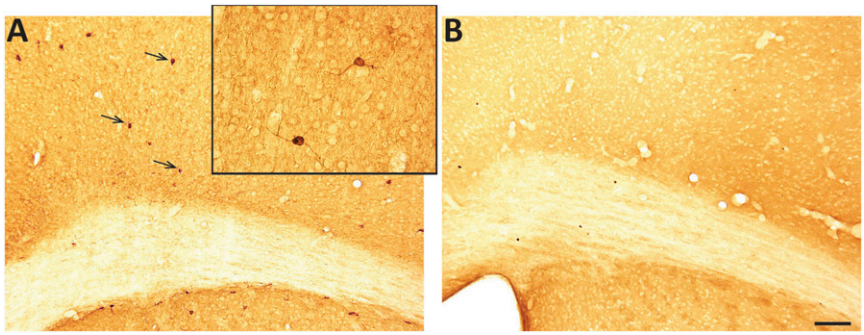

Fig. S6. Histological confirmation of genotypes. (*A*) Section containing the cerebral cortex (*Upper*) and striatum (*Lower*) from a WT mouse brain immunostained for nNOS. Arrows indicate representative nNOS-immunoreactive neurons. (*Inset*) nNOS-immunoreactive cortical neurons at higher magnification. (*B*) Similar section from an nNOS KO mouse that was immunostained in parallel with the section illustrated in *A*. No immunoreactive neurons were found in these mice. (Scale bar, 100 μM.)

Table S1. Sleep/wake parameters during the final 90 min in the 15 groups of rats reported in the current study

Duration of SD (h)	Duration of RS (h)	Time of killing	*n*	%Fos/nNOS	Wake (min)	NREM (min)	REM (min)	Normalized NRD	Normalized NRDE
Protocol 1									
0	0	ZT4	5	21.6	39.5 ± 7.4	41.4 ± 5.7	9.1 ± 2.2	1.12 ± 0.08	0.74 ± 0.15
0	0	ZT6	4	19.1	37.2 ± 7.9	42.8 ± 6.9	10.1 ± 1.2	0.92 ± 0.05	0.67 ± 0.14
0	0	ZT8	4	6.3	33.0 ± 2.3	47.5 ± 3.1	9.5 ± 1.9	0.99 ± 0.16	0.78 ± 0.13
0	0	ZT9	4	4.8	26.9 ± 2.9	48.6 ± 2.5	14.5 ± 1.0	0.89 ± 0.18	0.73 ± 0.17
0	0	ZT10	8	2.4	34.2 ± 4.3	45.0 ± 3.5	10.8 ± 0.9	0.70 ± 0.08	0.54 ± 0.09
Protocol 2									
2	2	ZT4	5	38.7	41.3 ± 12.2	43.7 ± 10.7	5.0 ± 1.9	1.41 ± 0.13	0.86 ± 0.26
2	4	ZT6	2	39.6	13.3 ± 3.1	66.0 ± 0.7	10.7 ± 2.4	1.37 ± 0.43	1.51 ± 0.46
4	2	ZT6	3	81.5	14.9 ± 3.6	66.9 ± 3.2	8.2 ± 0.5	1.75 ± 0.23	1.97 ± 0.35
Protocol 3									
6	0	ZT6	4	2.7	88.9 ± 0.6	1.1 ± 0.6	0 ± 0	0.86 ± 0.15	0.02 ± 0.01
6	0.5	ZT6.5	6	9.0	73.5 ± 4.6	13.9 ± 3.6	2.6 ± 1.1	1.65 ± 0.14	0.38 ± 0.10
6	1	ZT7	6	43.0	44.4 ± 3.2	38.3 ± 3.2	7.3 ± 0.9	1.64 ± 0.14	1.06 ± 0.15
6	1.5	ZT7.5	6	63.6	28.7 ± 4.6	48.9 ± 2.7	12.4 ± 2.1	1.97 ± 0.17	1.66 ± 0.16
6	2	ZT8	6	65.9	11.8 ± 1.9	64.4 ± 2.1	14.1 ± 0.6	1.72 ± 0.25	1.84 ± 0.26
6	3	ZT9	6	62.8	19.6 ± 3.0	61.4 ± 2.4	9.0 ± 1.0	1.34 ± 0.12	1.39 ± 0.16
6	4	ZT10	6	54.3	22.6 ± 2.6	56.3 ± 2.1	11.1 ± 1.2	1.27 ± 0.07	1.20 ± 0.08

All values are mean ± SEM.